AIAA JOURNAL
Vol. 43, No. 7, July 2005

Hypersonic Flow Simulation by the Gas-Kinetic Bhatnagar–Gross–Krook Scheme

Ong J. Chit*
University Technology MARA, Penang 13500, Malaysia
Ashraf A. Omar† and Waqar Asrar‡
International Islamic University Malaysia, Kuala Lumpur 53100, Malaysia
and
Zairil A. Zaludin§
University Putra Malaysia, Selangor 43400, Malaysia

The gas-kinetic Bhatnagar–Gross–Krook (BGK) scheme is extended to hypersonic flow simulations and thus shows that the compressible inviscid flow solutions of the simulations are efficiently and accurately obtained from the BGK scheme without the disastrous shock instability phenomenon that occurs in most hypersonic flow simulations involving strong shock waves. For this particular study, the effect of chemistry in hypersonic flows has not been taken into account. Hence, the assumption of calorically perfect gas is imposed in all simulations. The high-order resolution of the scheme is achieved by utilizing monotone upstream-centered schemes for conservation laws-type initial reconstruction. While, an implicit-type time-integration method known as the approximate factorization–alternating direction implicit is adopted for computing both steady and unsteady calculations. The gas-kinetic scheme is tested meticulously in four two-dimensional numerical examples, namely, the blunt-body problem, the double Mach reflection problem, the axisymmetric blunt-body problem, and the flow over a 15-deg ramp. The numerical results of the BGK scheme when compared with the other schemes and experimental data show that this numerical technique is robust, accurate, and stable for hypersonic flow.

Nomenclature

$\hat{A}, \hat{B}$	=	flux Jacobian matrices
C_p	=	pressure coefficient
$d\Xi$	=	volume element
F, G	=	inviscid flux vector
f, g	=	particle distribution function
I	=	identity matrix
J	=	Jacobian of transformation
P	=	pressure
Q	=	primitive variable
R	=	flux residual
t	=	time
U, V	=	macroscopic velocity components
u, v	=	microscopic velocity components
W	=	conservative variable
$\hat{W}, \hat{F}, \hat{G}$	=	transformed vector
x, y	=	Cartesian coordinates
γ	=	specific heat ratio
Δt	=	time step
ε	=	total energy
λ	=	function of pressure and density
ξ, η	=	generalized coordinates
ρ	=	density
ς	=	internal degree of freedom
τ	=	collision time
ϕ	=	van Leer's limiter
φ	=	adaptive parameter
Ψ	=	moment vector

Received 28 May 2004; revision received 21 November 2004; accepted for publication 19 March 2005.

*Lecturer, Faculty of Mechanical Engineering, Permatang Pauh.
†Associate Professor, Department of Mechanical Engineering, Jalan Gombak. Associate Member AIAA.
‡Professor, Department of Mechanical Engineering, Jalan Gombak.
§Lecturer, Department of Aerospace Engineering, Serdang. Member AIAA.

I. Introduction

TREMENDOUS efforts have been devoted and great progress has been achieved in the field of computational fluid dynamics of hypersonic flows in the past decade.[1–4] An evident achievement in this field is the development of the numerical scheme for spatial discretization. Currently, the most notable and successful numerical flux function for high-speed flow computations belongs to the upwind difference schemes because of their superior accuracy. The flux-difference-splitting (FDS) framework is one of the most successful groups among the upwind difference schemes that is widely used and studied. The Roe's FDS scheme,[5] for instance, is the most popular owing to its accuracy for compressible inviscid and viscous flow simulations. However, the occurrence of transverse shock instability and negative internal energy limits its usage in the computation of high-speed flows with strong shock waves and expansion fans.[6] This is supported by the findings of Peery and Imlay[7] for blunt-body computations with Roe's FDS, which produce the carbuncle phenomenon. This phenomenon is a numerical instability that occurs when capturing a strong shock wave in multidimensional computation. In addition to the FDS schemes, another group of upwind difference schemes, namely, the flux-vector-splitting (FVS) schemes can lack the robustness, accuracy, and efficiency in comparison to the FDS schemes. It is well known that FVS schemes have a large numerical dissipation on contact discontinuities, which explains the reason for their poor shock resolution capability at contact discontinuities.[8]

The development of gas-kinetic schemes has attracted much attention in recent years. These schemes are based on the approximate collisional Boltzmann equation.[9,10] A particular strength of the kinetic schemes lies precisely where FDS schemes often fail, such as carbuncle phenomenon, entropy condition, and positivity.[11–13] There are mainly two kinds of gas-kinetic schemes, and the differences lie within the governing equations used in the gas evolution stage. One of the well-known kinetic schemes is called the

kinetic flux vector splitting (KFVS), which is based on the collisionless Boltzmann equation, and the other is based on the collisional Bhatnagar–Gross–Krook (BGK) model.[14,15] Like any other FVS method, the KFVS scheme is very diffusive and less accurate in comparison with the Roe-type FDS method. The diffusivity of the FVS schemes is mainly caused by the particle or wave-free transport mechanism, which sets the Courant–Friedrichs–Lewy (CFL) time step equal to particle collision time.[16] To reduce diffusivity, particle collisions have to be modeled and implemented into the gas evolution stage. One of the distinct approaches to take particle collision into consideration in gas evolution can be found in Xu.[9] In this method, the collision effect is considered by the BGK model as an approximation of the collision integral in the Boltzmann equation. It is found that this gas-kinetic BGK scheme possesses accuracy that is superior to the flux-vector-splitting schemes and avoids the anomalies of FDS-type schemes.[6,9,11,17,18]

The paper is organized as follows. In Sec. II, the governing compressible Euler equations for two-dimensional flow expressed in both Cartesian and generalized coordinates are presented. In the subsequent section, the numerical formulation of the gas-kinetic BGK scheme and the proper way of extending the scheme to higher-order accuracy via the monotone upstream-centered schemes for conservation laws (MUSCL) interpolation technique will be addressed. Then, an implicit time-integration method is applied on the formulated BGK scheme. In Sec. IV, the kinetic scheme is applied to four hypersonic flow numerical examples. The results produced are highly stable and accurate at high speed with strong shock waves. The last section provides the conclusions.

II. Governing Equations

The two-dimensional compressible Euler equations expressed in Cartesian coordinates are written as

$$\frac{\partial W}{\partial t}+\frac{\partial F}{\partial x}+\frac{\partial G}{\partial y}=0 \tag{1}$$

where

$$W=\begin{bmatrix}\rho\\ \rho U\\ \rho V\\ \rho\varepsilon\end{bmatrix},\qquad F=\begin{bmatrix}\rho U\\ \rho U^2+p\\ \rho UV\\ (\rho\varepsilon+p)U\end{bmatrix},\qquad G=\begin{bmatrix}\rho V\\ \rho UV\\ \rho V^2+p\\ (\rho\varepsilon+p)V\end{bmatrix} \tag{2}$$

In Eq. (1), ρ, ρU, ρV, and $\rho\varepsilon$ are the macroscopic mass, x momentum, y momentum, and total energy density respectively, and p is the pressure.

Using eq. (1), when transformed from Cartesian coordinates (x, y) to generalized coordinates (ξ, η), the following form is obtained:

$$\frac{\partial \hat{W}}{\partial t}+\frac{\partial \hat{F}}{\partial \xi}+\frac{\partial \hat{G}}{\partial \eta}=0 \tag{3}$$

where

$$\hat{W}=J^{-1}W,\qquad \hat{F}=J^{-1}(\xi_x F+\xi_y G)$$
$$\hat{G}=J^{-1}(\eta_x F+\eta_y G) \tag{4}$$

In Eq. (4), $J=(\xi_x\eta_y-\xi_y\eta_x)$ is the Jacobian of transformation. The manner in which the metrics ξ_x, ξ_y, η_x, η_y and the Jacobian of transformation J are evaluated is detailed in Hoffmann and Chiang.[19]

III. Numerical Methods

A. Gas-Kinetic BGK Scheme

The BGK model in the two-dimensional case is[9]

$$\frac{\partial f}{\partial t}+u\frac{\partial f}{\partial x}+v\frac{\partial f}{\partial y}=\frac{(g-f)}{\tau} \tag{5}$$

where f is the real particle distribution function and g is the equilibrium state approached by f within a collision timescale τ. Both f and g are functions of space x, y; time t; particle velocity u, v; and internal degrees of freedom ς.

The equilibrium state g in the two-dimensional BGK model for the Euler equations is the Maxwell–Boltzmann distribution function and has the following form:

$$g=\rho(\lambda/\pi)^{(K+2)/2}\exp\{-\lambda[(u-U)^2+(v-V)^2+\varsigma^2]\} \tag{6}$$

where U and V are the macroscopic velocities in x and y directions, λ is a function of density and pressure $\lambda=\rho/2p$, and ς is a K-dimensional vector that accounts for the internal degrees of freedom such as molecular rotation, translation, and vibration. The dimensional vector K is related to the specific heat ratios and the space dimension by the relation $K=(4-2\gamma)/(\gamma-1)$, where for a diatomic gas $\gamma=1.4$.

The relations between the densities of mass ρ, momentum $(\rho U, \rho V)$, and total energy ε with the distribution function f are derived from the following moment relation:

$$\begin{pmatrix}\rho\\ \rho U\\ \rho V\\ \varepsilon\end{pmatrix}=\int f\Psi\,\mathrm{d}\Xi \tag{7}$$

where $\mathrm{d}\Xi=\mathrm{d}u\,\mathrm{d}v\,\mathrm{d}\varsigma$ is the volume element in the phase space and Ψ is the vector of moments given as

$$\Psi=\begin{pmatrix}1\\ u\\ v\\ \frac{1}{2}(u^2+v^2+\varsigma^2)\end{pmatrix} \tag{8}$$

With the moment relation defined in Eq. (7), a similar approach could be adopted in obtaining the numerical fluxes across cell interfaces, and they are given as

$$F_x=\int uf\Psi\,\mathrm{d}\Xi,\qquad G_y=\int vf\Psi\,\mathrm{d}\Xi \tag{9}$$

where F_x and G_y are the physical flux in the x and y direction, respectively.

A general solution f of Eq. (5) at the cell interface $(x_{i+1/2}, y_j)$ in two-dimensions is obtained as[18]

$$f(0,0,t,u,v,\varsigma)=(1-\varphi)g_o+\varphi f_o(-ut,-vt) \tag{10}$$

where $\varphi=e^{-t/\tau}$ is an adaptive parameter. For a first-order scheme φ can be fixed in the numerical calculations. When the BGK scheme is extended to high order, the value of φ should depend on the real flow situations. This option is necessary to prevent numerical oscillations and physically correct in that it accounts for the nonequilibrium behavior of the gas flow in the discontinuity region. A possible choice for φ in a high-order scheme is to design a pressure-based stencil, such as the switch function in the Jameson–Schmidt–Turkel scheme.[9,16,18] However, the value of φ for the higher-order BGK scheme is fixed in this study.

Finally, the gas-kinetic BGK numerical flux across the cell interface in the x direction can be computed as

$$F_x=\int uf(0,0,t,u,v,\varsigma)\Psi\,\mathrm{d}\Xi,\qquad F_x=(1-\varphi)F_x^e+\varphi F_x^f \tag{11}$$

where F_x^e is the equilibrium flux function and F_x^f is the nonequilibrium or freestream flux function.

The numerical flux for the BGK scheme at the cell interface in the x direction is obtained from Eq. (11) as

$$F_{i+\frac{1}{2},j}=(1-\varphi)F^e_{i+\frac{1}{2},j}+\varphi F^f_{i+\frac{1}{2},j} \tag{12}$$

and the numerical flux at the cell interface in the y direction is obtained in a similar manner, and the resulting relation is presented as

$$G_{i,j+\frac{1}{2}} = (1-\varphi)G^{e}_{i,j+\frac{1}{2}} + \varphi G^{f}_{i,j+\frac{1}{2}} \tag{13}$$

B. Reconstruction Stage

For high-order spatial accuracy, a method known as the MUSCL approach[8] is adopted. To avoid spurious oscillations in the solution, a limiter is used to extrapolate the primitive variables at the cell interfaces. In this study, van Leer's limiter is employed. Hence, the left and right states of the primitive variables ρ, U, V, p at a cell interface could be obtained through the nonlinear reconstruction of the respective variables and are given as

$$Q_l = Q_{i,j} + \frac{1}{2}\phi\left(\frac{\Delta Q_{i+\frac{1}{2},j}}{\Delta Q_{i-\frac{1}{2},j}}\right)\Delta Q_{i-\frac{1}{2},j}$$

$$Q_r = Q_{i+1,j} - \frac{1}{2}\phi\left(\frac{\Delta Q_{i+\frac{3}{2},j}}{\Delta Q_{i+\frac{1}{2},j}}\right)\Delta Q_{i+\frac{1}{2},j} \tag{14}$$

where the subscripts l and r correspond to the left and right sides of a considered cell interface. In addition, $\Delta Q_{i+1/2,j} = Q_{i+1,j} - Q_{i,j}$. The van Leer's limiter used in the reconstruction of flow variables in Eq. (14) is given as

$$\phi(\Omega) = (\Omega + |\Omega|)/(1+\Omega) \tag{15}$$

By using the extrapolation relations in Eq. (15), a second-order spatial accurate scheme is produced.

C. Implicit Time-Integration Method

An implicit method known as the approximate-factorization–alternating-direction-implicit (AF-ADI) scheme is employed for all computations in this study. When applying the Euler backward time discretization for the AF-ADI method, the governing equations in the computational domain are given as

$$\left\{I + \Delta t\left[\frac{\partial}{\partial\xi}(\hat{A}^{+}+\hat{A}^{-}) + \frac{\partial}{\partial\eta}(\hat{B}^{+}+\hat{B}^{-})\right]\right\}^{n}\Delta\hat{W}_{i,j} = -R^{n}_{i,j}$$

$$R^{n}_{i,j} = \Delta t\left\{\frac{\partial\hat{F}}{\partial\xi} + \frac{\partial\hat{G}}{\partial\eta}\right\}^{n}_{i,j} \tag{16}$$

where R denotes a residual vector and $\Delta\hat{W}_{i,j} = \hat{W}^{n+1}_{i,j} - \hat{W}^{n}_{i,j}$. The flux Jacobians denoted by $\hat{A} = \partial\hat{F}/\partial\hat{W}$ and $\hat{B} = \partial\hat{G}/\partial\hat{W}$ in Eq. (16) can be taken as the Jacobian from van Leer's flux. These are given in Pulliam.[20] The left-hand side of Eq. (16) can be efficiently inverted by using the AF-ADI method.[21]

IV. Results and Discussion

Here the solutions of four two-dimensional numerical examples of hypersonic flow are presented. The computed results of the BGK scheme are compared with available experimental data, verification data from literature, and also with numerical results of Roe's FDS scheme. The findings show that the BGK scheme gives better results than the Roe's FDS scheme in term of accuracy, robustness, and shock stability.

A. Case 1: Blunt Body

This first test case provides the opportunity to test the BGK scheme for any possible failure because of the carbuncle phenomenon. The carbuncle phenomenon for a hypersonic flow around a blunt body was first reported by Peery and Imlay.[7] For steady-state flow, a Godunov-type scheme admits a spurious solution in which a protuberance grows ahead of the bow shock along the stagnation streamline. However, before going any further, one has to ascertain

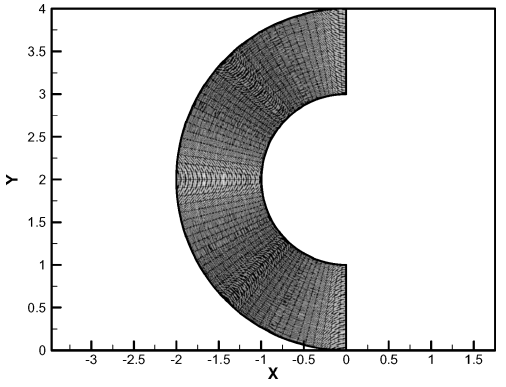

Fig. 1 Physical configuration for the blunt body.

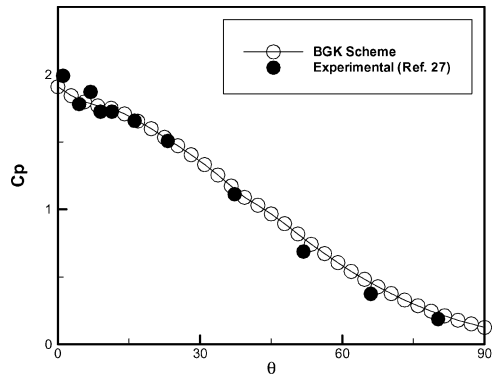

Fig. 2 Wall-pressure coefficient distributions for BGK scheme and experimental data.

that the computational results of the numerical schemes are physically correct and accurate. Thus, an initiative is taken here initially by validating the schemes with a test case that has experimental data. Hence, the blunt body will be tested with two sets of flow conditions, that is, the first condition is used for validation with the experimental data and the second condition is used for studying the carbuncle phenomenon of the hypersonic flow around blunt body.

The mesh size used for this problem is 65×113, and the geometry is shown in Fig. 1. For validating the numerical schemes, Lee[22] provided sets of measurements in hypersonic flows around a blunt body, which remain fully laminar and low enthalpy flow. These data can be used efficiently to examine the accuracy of numerical scheme itself because the uncertainties caused by turbulence and chemical reactions are excluded. The following flow conditions are chosen for generating numerical data:

$$M_\infty = 15.622, \quad \alpha = 0 \text{ deg}, \quad \rho_\infty = 1.814 \times 10^{-3} \text{ kg/m}^3$$

$$U_\infty = 2108.61 \text{ m/s}, \quad P_\infty = 23.622 \text{ N/m}^2$$

The numerical schemes for this typical problem are implemented at second-order accuracy and at CFL number of 1.0 with the AF-ADI method. The iterations were carried out until steady-state solution is reached. Figure 2 shows the computed pressure coefficient C_p distributions along the wall surface of the blunt body in clockwise direction, starting from the stagnation point. It contains the distributions for the BGK scheme without the Roe scheme simply because the Roe scheme failed to produce results for this problem if implemented without any boundary-layer corrections. From Fig. 2, it is observed that the BGK scheme is able to predict accurately the wall-pressure coefficient as validated by the experimental data of Lee.[22] In addition, Fig. 3, which is obtained from Lee,[22] is also included to further demonstrate the computational capabilities of the BGK scheme. When comparing the results of Fig. 2 with Fig. 3, one can deduce that the BGK scheme is as accurate as or better than the numerical schemes employed in Lee.[22] The reasoning behind this claim is that the numerical results of Fig. 3 are produced

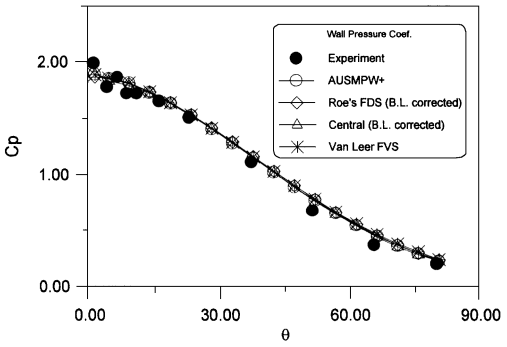

Fig. 3 Wall-pressure coefficient distributions from Lee.[22]

by compressible viscous flow algorithms, and some schemes even employed boundary-layer corrections in order to get satisfactory results.

To study the shock instabilities that occur in hypersonic flow for a blunt body, a second set of flow conditions is proposed as follows: freestream Mach number of 8.0 and at 0-deg incident angle. The boundary conditions for this problem are set as follows: the outer boundary of the domain, which is located away from the blunt body is set at the freestream; the boundaries that are located far downstream at the top and bottom of the blunt body, where the flow is supersonic, and extrapolation is used; and finally, the boundary condition at the blunt body itself is set by using the slip wall condition.

Again, the BGK scheme is implemented with similar criterion as stated as just stated. Figure 4a shows the pressure contour and the distribution of pressure along the stagnation line of a half-cylinder for the BGK scheme. Similarly, the numerical results for the second-order Roe's FDS scheme are presented in Fig. 4b. When the numerical results of these two schemes as depicted in Figs. 4a and 4b are compared to the numerical results from Kim et al.,[23] which are shown in Fig. 4c, it is obvious that the BGK scheme is superior to the Roe scheme. The Roe scheme produced numerical solutions with the occurrence of the so-called carbuncle phenomenon. Unsymmetrical flow behavior and the protuberance of the bow shock can be clearly seen in Fig. 4b. This shock instability phenomenon is not present within the BGK scheme, where the scheme is able to produce numerical results that are as accurate and stable as the shock-stable Roe scheme. In addition, the BGK scheme is able to produce excellent numerical results without any need of modifying the flux function as done by the shock-stable Roe scheme in order to avoid the occurrence of shock instabilities at high-speed flows. This implies that the BGK scheme itself is intrinsically robust and stable.

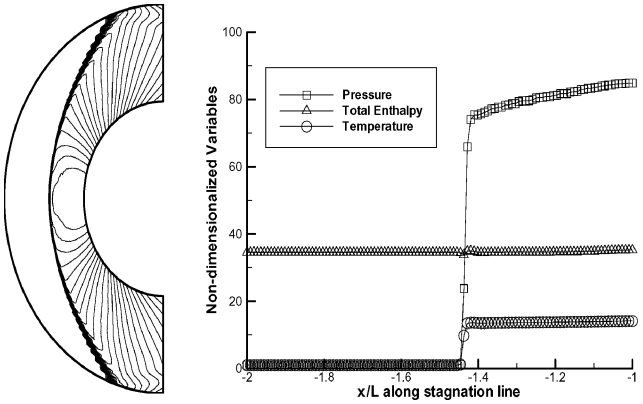

a) Second-order BGK scheme

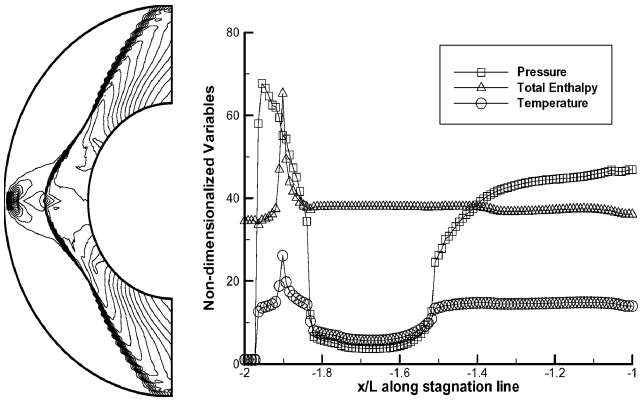

b) Second-order Roe scheme

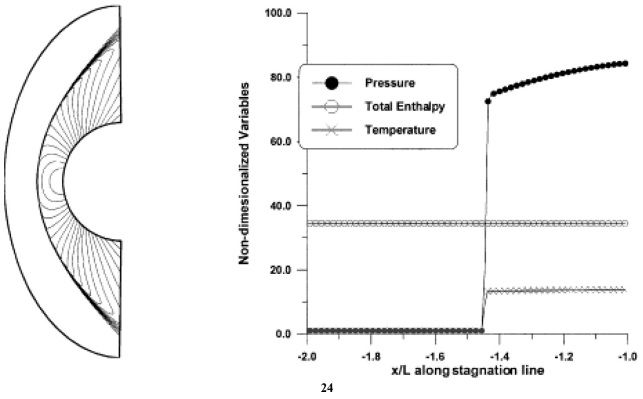

c) Shock-stable Roe scheme from Kim et al.[23]

Fig. 4 Pressure contours and distributions for blunt body along the stagnation line at $M_\infty = 8$ and 0-deg angle of attack.

B. Case 2: Double Mach Reflection

This numerical example is a classical test example dating at least back to the famous paper of Woodward and Collela.[24] It has been used extensively in the literature as a test case. It considers the reflection of a planar Mach shock in air from a wedge.

The computational domain is $[0,4] \times [0,1]$ with a mesh size of 481×121, and the reflecting wall lies at the bottom of the computational domain for $\frac{1}{6} \le x \le 4$. Initially, the right moving Mach 10 shock is positioned at $x = \frac{1}{6}$, $y = 0$, and makes a 60-deg angle with the x axis and extends to the top of the problem domain at $y = 1$. The short region from $x = 0$ to $\frac{1}{6}$ along the bottom boundary is always assigned values for the initial postshock flow. The left-hand boundary is also assigned with the initial postshock values, and at the right-hand boundary all gradients are set to zero. At the top boundary, the flow values are set to describe the exact motion of the Mach 10 shock. The undisturbed air ahead of the shock has a density of 1.4 and a pressure of 1.

The flow is computed using the first- and second-order BGK scheme with AF-ADI method for time integration at CFL number of 0.9. The problem was run until $t = 0.2$. The density and pressure contours with 30 equally spaced contour lines are plotted and shown in Figs. 5a and 5b, respectively, for the first-order BGK scheme and in Figs. 6a and 6b, respectively, for the first-order Roe scheme for region between $x = 0$ and 3. From these figures, the density and pressure contours for the first-order Roe scheme experienced the so-called kinked Mach phenomenon in comparison to the first-order BGK scheme, which is free from this sort of shock instability behavior. The kinked Mach phenomenon suffered by the Roe's FDS scheme has been reported by many numerical experimentations.[9,23,25] The numerical results of the second-order BGK scheme for the density and pressure contours are also plotted in Figs. 7a and 7b, respectively. The formation of the double Mach stems are captured accurately by the BGK scheme, which are very difficult to compute accurately.[24,26] In addition, the respective density and pressure contours for the second-order Roe scheme are also depicted in Figs. 8a and 8b. The outcome of the second-order Roe scheme is somehow satisfactory in comparison with its first-order results. Through the numerical results obtained, it is substantiated

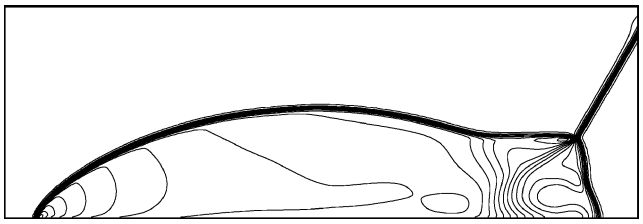

a) Density contours

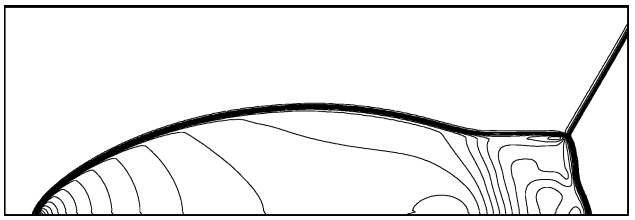

b) Pressure contours

Fig. 5 Double Mach reflection by first-order BGK scheme, $M_{\text{shock}} = 10$.

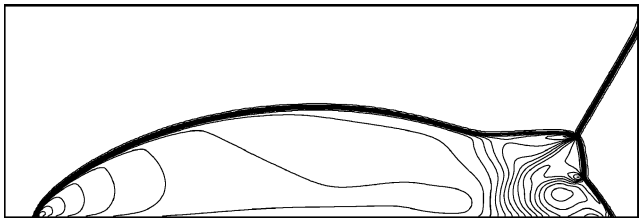

a) Density contours

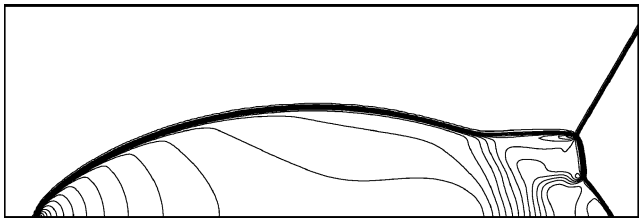

b) Pressure contours

Fig. 6 Double Mach reflection by first-order Roe scheme, $M_{\text{shock}} = 10$.

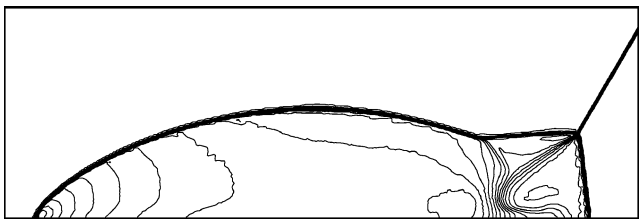

a) Density contours

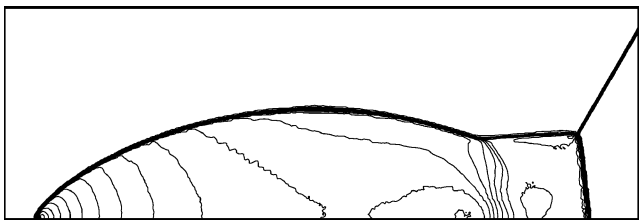

b) Pressure contours

Fig. 7 Double Mach reflection by second-order BGK scheme, $M_{\text{shock}} = 10$.

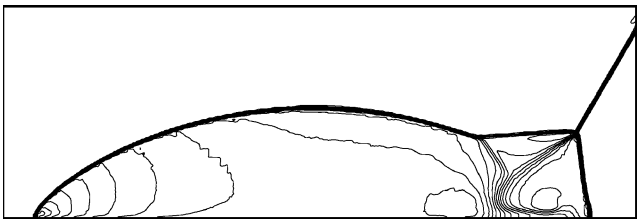

a) Density contours

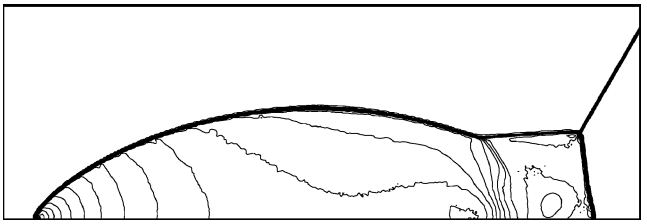

b) Pressure contours

Fig. 8 Double Mach reflection by second-order Roe scheme, $M_{\text{shock}} = 10$.

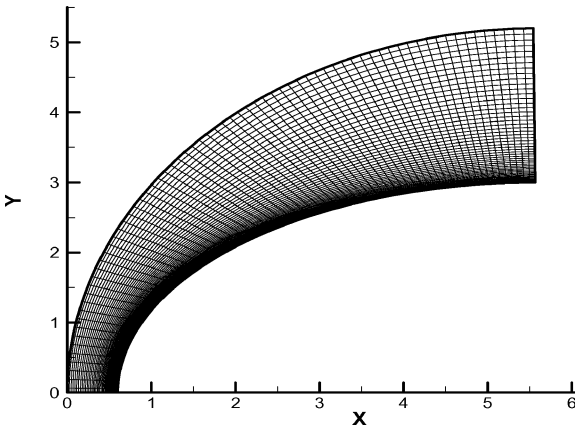

Fig. 9 Physical configuration for the axisymmetric blunt body.

that the BGK scheme is more robust and superior to the Roe's FDS scheme in terms of shock stability at high-speed flow. The excellent computational characteristics of the BGK scheme over the Roe scheme are evident via the facts that the BGK scheme is able to generate the solutions without causing any kinked Mach for both first- and second-order accuracy. However, the Roe scheme is only able to produce satisfactory results at second-order accuracy.

C. Case 3: Axisymmetric Blunt Body

This test case is taken from a numerical application found in Hoffmann and Chiang.[21] Because the flow considered for this typical problem is two-dimensional axisymmetric flow, the governing equations are not the two-dimensional planar Euler equations as dictated in Eqs. (1) and (3). Instead, the axisymmetric Euler equations as described in Hoffmann and Chiang[21] are used as the corresponding governing equations.

The physical domain of this problem is shown in Fig. 9 with a mesh size of 71×53. A freestream Mach number of 18 is used to initialize the flowfield at zero angle of attack. The four boundaries of the axisymmetric blunt body consist of an outer boundary, which is set at freestream conditions: a boundary along the stagnation line, which is set with symmetry condition; an outflow boundary at far downstream of the domain where extrapolation is used; and an inviscid solid wall at the inner boundary.

This flow is computed using the second-order BGK scheme with AF-ADI as the time-integration method at CFL = 1.0. The solution is obtained after 1000 iterations when steady state is achieved. The pressure contours of the BGK scheme and the Roe scheme are depicted in Figs. 10a and 10b, respectively, and the pressure

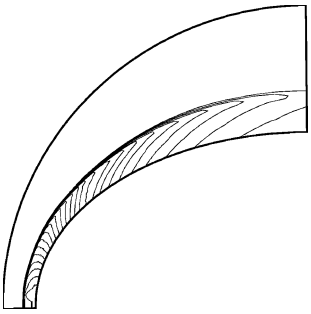

a) Second-order BGK scheme

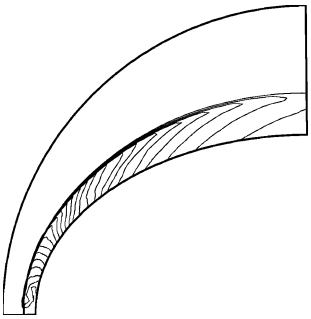

b) Second-order Roe scheme

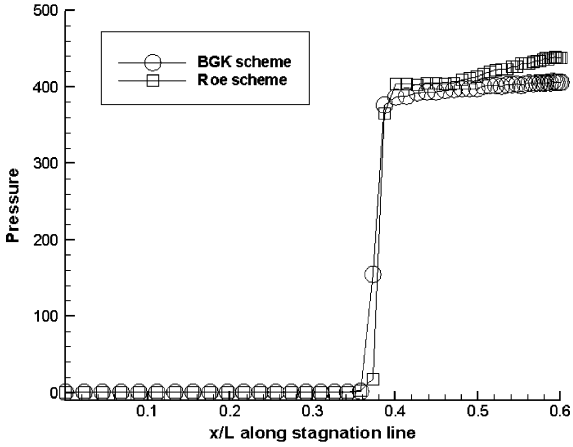

c) Pressure distribution for second-order BGK and second-order Roe schemes

Fig. 10 Pressure contours and distributions for axisymmetric blunt body along the stagnation line at $M_\infty = 18$ and 0-deg angle of attack.

distributions plot comparing the two schemes is shown in Fig. 10c. The contour plots from the BGK and Roe scheme are in agreement with each other and with the results of Hoffmann and Chiang.[21] Comparing the pressure distributions along the stagnation line for the two schemes, they show that the solutions provided by the Roe scheme after the bow shock are not as smooth as the BGK scheme. This again indicates that the BGK scheme is better than the Roe scheme in terms of flow resolution for hypersonic flows.

D. Case 4: Hypersonic Ramp

This numerical example studies the Mach 7 flow over a 15-deg ramp, and it is taken from Slater.[27] The computations carried out by Slater[27] in his study use the Navier–Stokes equations. However, in this study the flow problem will be used as a platform to test the compressible Euler equations flow solver, namely, the BGK scheme. This study is feasible because at hypersonic speed and at low angle of attack the viscosity effects of the flow can be considered as negligible.

For this study, a single-block, two dimensional H-grid with mesh size of 151 × 101 is used. The grid is shown in Fig. 11. The flow is initialized with a uniform flow at freestream Mach number of 7 at

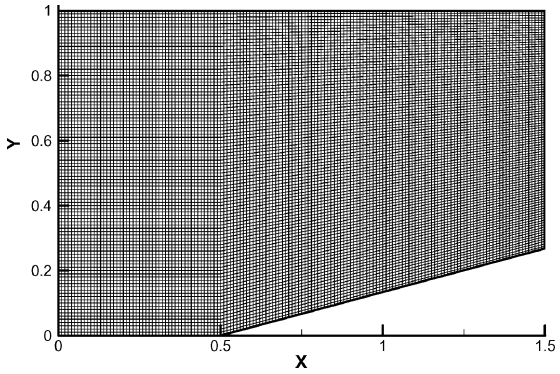

Fig. 11 Grid for the hypersonic ramp.

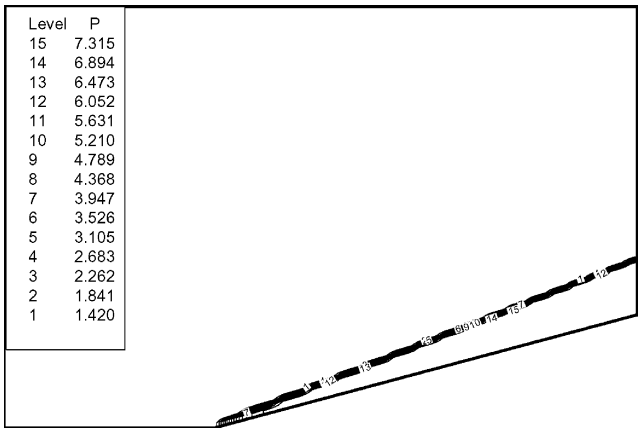

a) Second-order BGK scheme

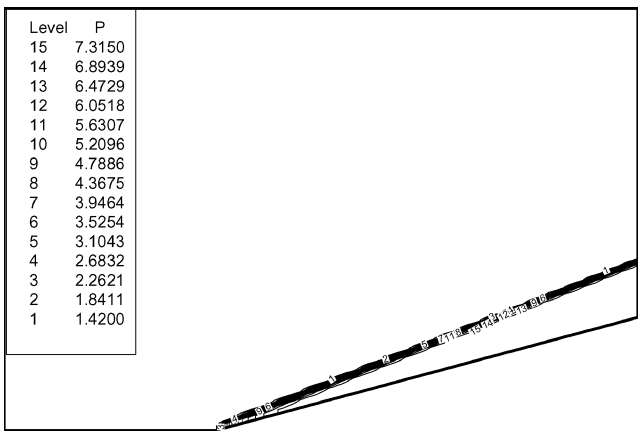

b) Second-order Roe scheme

Fig. 12 Pressure contours for the hypersonic ramp at $M_\infty = 7$ and 0-deg angle of attack.

zero angle of attack. At the inlet where the inflow condition is above Mach 1.0, the boundary is specified as frozen boundary. Because the outlet of the computational domain is supersonic, an extrapolation method of flow variables is prescribed. While at the upper and the lower boundaries of the ramp, where the boundaries are solid walls, an inviscid wall condition is used.

This solution is computed using the second-order BGK scheme with an AF-ADI time-integration method. The CFL number used is 1.0. The computations are carried out until steady state is reached. The computed pressure contours for the BGK and Roe schemes are shown in Figs. 12a and 12b, respectively. They show good agreement with each other and with the contour plot of Slater.[27] The pressure distributions of the two schemes along the lower wall boundary of the ramp are compared with each other and with the distribution from Slater.[27] This is shown in Fig. 13. From this figure, one can see

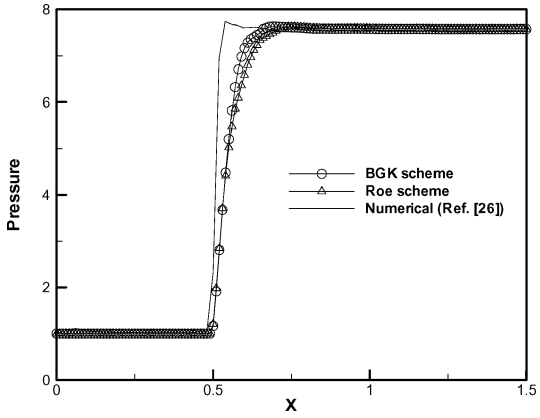

Fig. 13 Comparison of pressure distributions for the hypersonic ramp by the second-order BGK and Roe schemes with numerical results from Slater.[27]

that the BGK and the Roe schemes are able to capture the location of the shock at $x = 0.5$ more accurately than Slater.[27] In addition, the shock resolution capability presented by the BGK scheme is better in comparison to the Roe scheme as evident in Fig. 13. Finally, the numerical results obtained for this study verify our previous assumptions that at very high speed and at low angle of attack the viscosity effect is negligible for a calorically perfect gas.

V. Conclusions

The Bhatnagar–Gross–Krook (BGK) scheme is successfully extended to the simulation of two-dimensional compressible inviscid flow at hypersonic speeds in the present paper. Four distinct numerical examples have been tested with the BGK scheme and their numerical results verified. The first and second tests' outcomes show that the BGK scheme is very robust and stable in comparison to Roe's flux-difference-splitting scheme, where the Roe scheme encountered carbuncle and kinked Mach stem phenomenon. The carbuncle and the kinked Mach stem phenomenon that occur in the simulations are examples of shock instabilities that occur at hypersonic flows. The third and the fourth tests, namely, axisymmetric blunt body and hypersonic ramp, demonstrate that the BGK scheme is more accurate in comparison to the Roe scheme. Thus, this study concludes that the BGK scheme is able to produce numerical results with better accuracy, high-resolution capabilities to capture shock, rarefaction, and contact discontinuities as well as being robust and stable.

Acknowledgment

The authors acknowledge the support of the Research Center, International Islamic University Malaysia.

References

[1]Kim, S. S., Kim, C., and Rho, O. H., "Multigrid Algorithm for Computing Hypersonic, Chemically Reacting Flows," *Journal of Spacecraft and Rockets*, Vol. 38, No. 6, 2001, pp. 865–874.

[2]Lee, J. H., and Rho, O. H., "Numerical Analysis of Hypersonic Viscous Flow Around a Blunt Body Using Roe's FDS and AUSM+ Schemes," AIAA Paper 97-2054, June 1997.

[3]Lee, J. H., and Rho, O. H., "Accuracy of AUSM+ Scheme in Hypersonic Blunt Body Flow Calculations," AIAA Paper 98-1538, April 1998.

[4]Gnoffo, P. A., "Computational Fluid Dynamics Technology for Hypersonic Applications," AIAA Paper 2003-3259, July 2003.

[5]Roe, P. L., "Approximate Riemann Solvers, Parameter Vectors and Difference Schemes," *Journal of Computational Physics*, Vol. 43, No. 2, 1981, pp. 357–372.

[6]Chae, D. S., Kim, C. A., and Rho, O. H., "Development of an Improved Gas-Kinetic BGK Scheme for Inviscid and Viscous Flows," *Journal of Computational Physics*, Vol. 158, No. 1, 2000, pp. 1–27.

[7]Peery, K. M., and Imlay, S. T., "Blunt-Body Flow Simulations," AIAA Paper 88-2904, July 1988.

[8]Hirsch, C., *The Numerical Computation of Internal and External Flows*, Vol. 2, Wiley, New York, 1990, Chap. 21.

[9]Xu, K., "Gas-Kinetic Scheme for Unsteady Compressible Flow Simulations," von Kármán Inst. for Fluid Dynamics Lecture Series, Vol. 1998-03, Von Kármán Inst., Rhode St. Genese, Belgium, 1998, pp. 1–101.

[10]Ong, J. C., "Computational Analysis of Gas-Kinetic BGK Scheme for Inviscid Compressible Flow," M.S. Thesis, Dept. of Aerospace Engineering, Univ. Putra Malaysia, Selangor, Malaysia, 2004.

[11]Xu, K., "Gas Evolution Dynamics in Godunov-Type Schemes and Analysis of Numerical Shock Instability," ICASE, Rept. 99-6, Jan. 1999.

[12]Xu, K., and Lui, S., "Entropy Analysis of Kinetic Flux Vector Splitting Schemes for the Compressible Euler Equations," ICASE, Rept. 99-5, Jan. 1999.

[13]Tang, T., and Xu, K., "Gas-Kinetic Schemes for the Compressible Euler Equations I: Positivity-Preserving Analysis," *Zeitschrift fürAangewandte Mathematik und Physik*, Vol. 50, No. 2, 1999, pp. 258–281.

[14]Ong, J. C., Omar, A. A., and Asrar, W., "The Accuracy of Gas-Kinetic Schemes for Solving Inviscid Hypersonic Axisymmetric Blunt Body Problem," Engineering and Technology Conf. (EnTech), Sarawak, Malaysia, July 2003.

[15]Ong, J. C., Omar, A. A., Asrar, W., and Hamdan, M. M., "Development of Gas-Kinetic BGK Scheme for Two-Dimensional Compressible Inviscid Flows," AIAA Paper 2004-2708, June 2004.

[16]Xu, K., "Gas-Kinetic Theory Based Flux Splitting Method for Ideal Magnetohydrodynamics," ICASE, Rept. 98-53, Nov. 1998.

[17]Ong, J. C., Omar, A. A., and Asrar, W., "Evaluation of Gas-Kinetic Schemes for 1D Inviscid Compressible Flow Problem," *International Journal of Computational Engineering Science*, Vol. 4, No. 1, 2003, pp. 829–851.

[18]Ong, J. C., Omar, A. A., Asrar, W., and Hamdan, M. M., "An Implicit Gas-Kinetic BGK Scheme for Two-Dimensional Compressible Inviscid Flows," *AIAA Journal*, Vol. 42, No. 7, 2004, pp. 1293–1301.

[19]Hoffmann, K. A., and Chiang, S. T., *Computational Fluid Dynamics for Engineers*, Engineering Education System, Vol. 1, Wichita, KS, 1993, Chaps. 3 and 9.

[20]Pulliam, T. H., "Notes on Solution Methods in Computational Fluid Dynamics," NASA Ames Research Center, Moffett Field, CA, Jan. 1986.

[21]Hoffmann, K. A., and Chiang, S. T., *Computational Fluid Dynamics for Engineers*, Engineering Education System, Vol. 2, Wichita, KS, 1993, Chaps. 11 and 12.

[22]Lee, J. H., "Numerical Analysis of Hypersonic Shock-Shock Interaction Using AUSMPW+ Scheme," Ph.D. Dissertation, Dept. of Aerospace, Seoul National Univ., Seoul, Republic of Korea, Feb. 1999.

[23]Kim, S. S., Kim, C., and Rho, O. H., "Cures for the Shock Instability: Development of a Shock-Stable Roe Scheme," *Journal of Computational Physics*, Vol. 185, No. 2, 2003, pp. 342–374.

[24]Woodward, P., and Colella, P., "The Numerical Simulation of Two-Dimensional Fluid Flow with Strong Shocks," *Journal of Computational Physics*, Vol. 54, No. 1, 1984, pp. 115–173.

[25]Quirk, J. J., "A Contribution to the Great Riemann Solver Debate," *International Journal for Numerical Methods in Fluids*, Vol. 18, No. 6, 1994, pp. 555–574.

[26]Shi, J., Zhang, Y. T., and Shu, C. W., "Resolution of High Order WENO Schemes for Complicated Flow Structures," *Journal of Computational Physics*, Vol. 186, No. 2, 2003, pp. 690–696.

[27]Slater, J. W., "Hypersonic Ramp: Study #1," *NASA Glenn Research Center* [online database], URL, http://www.grc.nasa.gov/WWW/wind/valid/hypramp/hypramp01/hypramp01.html [cited 2 April 2004].

G. Candler
Associate Editor